5. EXPLANATORY NOTES[1]

Shipboard Scientific Party[2]

INTRODUCTION

This chapter is devoted to a description of the sampling, measurement, and core description procedures and methods used during Leg 158. It will help the reader understand the basis for our preliminary conclusions and also help the interested investigator select samples for further analysis. This chapter concerns only shipboard operations and analyses described in the site report in the *Initial Results* volume of the Leg 158 *Proceedings of the Ocean Drilling Program.* Methods used by various investigators for shore-based analysis of Leg 158 data will be detailed in individual papers published in the *Scientific Results* volume.

Site Report

Description of the drilling site, summaries of operations, and preliminary results are contained in the site report. The separate sections of the site report were written by the following shipboard scientists (authors are listed in alphabetical order; no seniority is implied):

Principal results: Herzig, Humphris
Operations: Miller, Pollard
Stratigraphy: Hannington
Sulfide petrology and geochemistry: Brown, Brügmann, Chiba, Fouquet, Gemmell, Hannington, Holm, Honnorez, Knott, Nakamura, Petersen, Tivey
Hydrothermal alteration: Alt, Honnorez
Igneous petrology and geochemistry: Alt, Honnorez, Smith
Physical properties: Becker, Iturrino, Ludwig, Rona
Paleomagnetism: Zhao
Fluid geochemistry: Sturz
Microbiology: Reysenbach

Summary core descriptions ("barrel sheets" and visual core descriptions for igneous, hydrothermally altered rocks, and sulfides) and photographs of each core appear in Section 3, and polished thin section sample descriptions appear in Section 4.

Shipboard Curation Procedures

Numbering of Site, Holes, and Cores

Drilling sites are numbered consecutively from the first site drilled by the *Glomar Challenger* in 1968. A site number refers to one or more holes drilled while the ship was positioned over one acoustic beacon. Multiple holes may be drilled at a single site by pulling the drill pipe above the seafloor (out of the hole), moving the ship some distance from the previous hole, and then drilling another hole. In some cases, the ship may return to a previously occupied site to drill additional holes.

For all Ocean Drilling Program (ODP) drill sites, a letter suffix distinguishes each hole drilled at the same site. For example, the first hole drilled is assigned the site number modified by the suffix A, the second hole takes the site number and suffix B, and so forth. Note that this procedure differs slightly from that used by the Deep Sea Drilling Project (DSDP) (Sites 1 through 624), but this prevents ambiguity between site- and hole-number designations. It is important to distinguish among holes drilled at a site because recovered sediments or rocks from different holes usually do not come from equivalent positions in the stratigraphic column.

The cored interval is measured in meters below seafloor (mbsf); sub-bottom depths are determined by subtracting the drill-pipe measurement (DPM) water depth (the length of pipe from the rig floor to the seafloor) from the total DPM (from the rig floor to the bottom of the hole; see Fig. 1). Echo-sounding data (from the precision depth recorders) are used to locate the site, but they are not used as a basis for any further measurements. Water depths are estimated from the length of drill pipe deployed measured from the rig floor, less the dis-

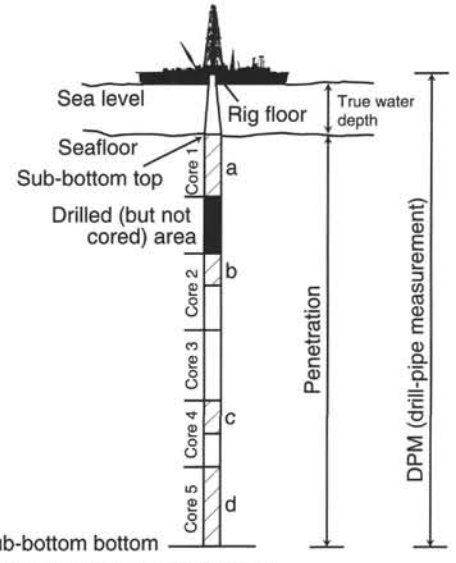

Figure 1. Diagram illustrating terms used in the discussion of coring operations and core recovery.

[1]Humphris, S.E., Herzig, P.M., Miller, D.J., et al., 1996. *Proc. ODP, Init. Repts.*, 158: College Station, TX (Ocean Drilling Program).

[2]Shipboard Scientific Party is as given in the list of participants in the contents.

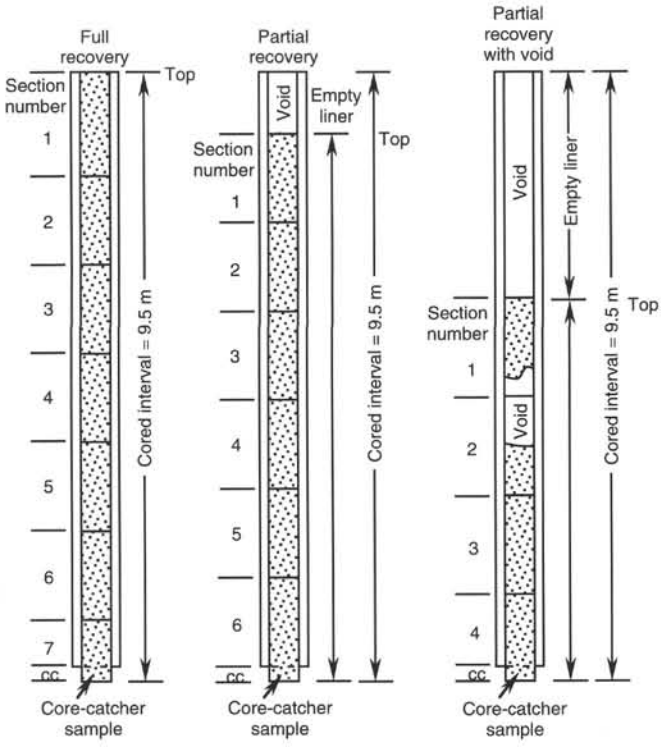

Figure 2. Diagram showing procedure used in cutting and labeling core sections.

tance from the rig floor to sea level. The rig-floor height varies from hole to hole and is reported in the summary tables of the site report.

The depth interval assigned to an individual core begins with the depth below the seafloor that the coring operation began and extends to the depth that the coring operation ended for that core (see Fig. 1). For rotary coring (RCB and XCB), each coring interval is equal to the length of the joint of drill pipe added for that interval (although a shorter core may be attempted in special instances). The drill pipe in use varies from about 9.4 to 9.8 m in length. The pipe is measured as it is added to the drill string, and the cored interval is usually recorded as the length of the pipe joint to the nearest 0.1 m. For hydraulic piston coring (APC) operations, the drill string is advanced 9.5 m after each core is taken, the maximum length of the piston stroke. Cored intervals may not necessarily be adjacent if separated by drilled intervals. In drilling hard rock, a center bit may replace the core barrel if it is desirable to drill without coring. For coring with the motor-driven core barrel (MDCB), the coring interval was taken as the distance into the formation that the MDCB advanced, which could be a maximum of 4.5 m.

Cores taken from a hole are numbered serially from the top of the hole downward. Core numbers and their associated cored intervals (in mbsf) are unique in a given hole. Maximum full recovery for a single core is 9.5 m of rock or sediment contained in a plastic liner (6.6 cm internal diameter) plus about 0.2 m (without a plastic liner) in the core catcher (Fig. 2). The core catcher is a device at the bottom of the core barrel that prevents the core from sliding out when the barrel is being retrieved from the hole.

All ODP core and sample identifiers indicate core type. The following abbreviations were used by Leg 158: R = rotary core barrel (RCB), N = motor-driven core barrel (MDCB), X = extended core barrel (XCB), B = drill-bit recovery, C = center-bit recovery, and W = wash core.

Core Handling

As soon as a core arrived on deck, the core was tested for H_2S and then placed on the long horizontal rack on the catwalk. H_2S emissions from the core were monitored through the use of stationary sensors on the rig floor, the catwalk, and in the core laboratory. In addition, local monitoring was performed on the rig floor and catwalk with hand-held, portable detectors. If excessive levels of H_2S are detected (>10 ppm), appropriate measures are taken (including clearing the affected area and allowing the gas to disseminate) to ensure the safety of the crew and the scientific party. No detectable levels of H_2S were measured during Leg 158.

Once on deck, the core catcher was placed at the bottom of the core liner, and total core recovery was calculated by shunting the sulfide and rock pieces together and measuring to the nearest centimeter. This information was then logged into the shipboard CORELOG database. Afterward, the core was cut into 1.5-m-long sections and transferred into the lab.

The contents of each section were transferred into 1.5-m-long sections of a split core liner, in which the bottoms of oriented pieces (i.e., pieces that clearly could not have rotated top to bottom about a horizontal axis in the liner) were marked with a red wax pencil. This ensures that orientation is not lost during the splitting and labeling process.

The 1.5-m sections were numbered serially from the top (Fig. 2). There are as many sections per core as necessary to accommodate the length of core recovered; for example, 4 m of core would be divided into two 1.5-m sections and one 1-m section. When, as is usually the case, the recovered core is shorter than the cored interval, the top of the core is equated with the top of the cored interval by convention, so as to achieve consistency in handling analytical data derived from the cores. In rare cases, a section less than 1.5 m may be cut to preserve features of interest (e.g., lithologic contacts).

In the core laboratory, scientists attempt to reconstruct pieces of the core that were fragmented during recovery. The core-catcher sample was placed at the bottom of the last section and was treated as part of the last section, rather than separately. In the event the only material recovered was in the core catcher, this sample was curated at the top of the cored interval. However, information supplied by the drillers or by other sources may allow for more precise interpretation as to the correct position of the core-catcher material within an incompletely recovered cored interval.

The core was then split into archive and working halves. A plastic spacer was used to separate individual pieces and/or reconstructed groups of pieces in the core liner. These spacers may represent a substantial interval of no recovery. Each piece was numbered sequentially from the top of each section, beginning with number 1; reconstructed groups of pieces were assigned the same number but were lettered consecutively. Pieces were labeled only on external surfaces. If the piece was oriented, an arrow was added to the label pointing to the top of the section.

A full identification number for a sample consists of the following information: leg, site, hole, core number, core type, section number, piece number (for hard rock), and interval in centimeters measured from the top of section. For example, a sample identification of "158-957A-5R-1, 10–12 cm" represents a sample removed from the interval between 10 and 12 cm below the top of Section 1, Core 5 (R designates that this core was taken during rotary coring) of Hole 957A during Leg 158.

The working half of the core was then sampled for shipboard laboratory studies. Records of all samples are kept by the curator at ODP. The archive half was described visually and photographed with both black-and-white and color film, one core at a time. Both halves of the core were then shrink-wrapped in plastic to prevent pieces from vibrating out of sequence during transit. The core halves were then placed in air-tight plastic/aluminum foil liners, evacuated, and

flushed with nitrogen. The cores were put into labeled plastic D-tubes, sealed, and transferred to cold-storage space aboard the drilling vessel. As with the other Leg 158 cores, they are housed under cold storage in the Bremen Core Repository.

STRATIGRAPHY

The data obtained during the shipboard analysis of each core were summarized in the core description forms or "barrel sheets" (Fig. 3). This information represents field notes taken on board ship. Because production schedules prohibit modification of the core description sheets with subsequent findings, occasional ambiguities or discrepancies may be present. The following discussion explains ODP conventions used to analyze cores and to prepare core description forms. Deviations from those procedures adopted by the Leg 158 Shipboard Scientific Party are also explained.

Visual core and thin-section descriptions provide the basic data used to prepare the core description forms. Identification of minerals by X-ray diffraction could not be conducted at sea, but a small number of samples were analyzed on shore post-cruise to augment descriptions of clay minerals.

Modified visual core description (VCD) forms that summarize the igneous, structural, and alteration features of the core on a section-by-section basis were used during Leg 158 (Figs. 3, 4). A photograph of the core section is spliced along the left side of the form for illustrative purposes. The left column of the form is a graphic representation of the archive half, drawn by scientists on board, then scanned into an electronic file for publication. Spacers between pieces are noted by a horizontal line across this column. Detailed sketches of individual pieces prepared during core description are also electronically scanned, annotated, and spliced onto the right side of the form. Oriented pieces are indicated by an up arrow in the column headed "Orientation." Shipboard samples are indicated in the column headed "Shipboard Studies" using the following notations: XRF = X-ray fluorescence analysis, XRD = X-ray diffraction analysis, TS = petrographic thin section, PM = paleomagnetic analysis, PP = physical properties analysis, AA = atomic absorption analysis, CM = Ca-Mg analysis, and REY = microbiology analysis. Lithologic units are designated in the next column, as defined in the "Sulfide Petrology and Geochemistry" section (this chapter). The column headed "Lithology" includes a graphic representation of the variation in lithologies downsection, with patterns defined in Figure 4. The right column includes structural summary symbols, as defined in Figure 4.

Textural descriptions of the core were recorded in the HARVI computerized database, or as ASCII text files for samples not accommodated by this software, and were spliced onto the right side of the VCD form for presentation in this volume. These electronic files are available from the ODP repositories.

SULFIDE PETROLOGY AND GEOCHEMISTRY

Introductory Comments

Mineralization in seafloor sulfide deposits can occur as massive sulfides, semi-massive sulfides, stockwork or stringer sulfides, sulfide-filled breccias, disseminated sulfides, and sulfide sediments. The manner in which they are curated, sampled, described, and analyzed overlaps procedures established for both igneous and hydrothermally altered rock (see "Hydrothermal Alteration" and "Igneous Petrology and Geochemistry" sections, this chapter). We consider sulfide deposits separately here because of the large range of lithologies, textures, and minerals observed during Leg 158 and because of the diversity of mineralization styles.

Core Curation and Shipboard Sampling

Sulfide cores were opened with a stainless steel knife, and the indurated pieces were cut with a rock saw. Cores were designated using leg, site, hole, core, section, and core type as discussed in the "Introduction" section (this chapter). Each section was examined, before being cut, for structural orientation, mineral textures, vein distribution, and hydrothermal alteration.

The archive half of each hard-rock sulfide core was described on a cruise-specific form, generally similar to that devised for igneous rocks (HARVI), and was photographed before storage. Close-up photographs were taken to illustrate representative structures and textures. During the core description process, samples were removed from the working half for analysis of physical and chemical properties. Nondestructive magnetic susceptibility measurements were made on whole cores, and thermal conductivity measurements were made on selected pieces of the core. The working half was sampled for shipboard polished thin sections, physical properties, magnetic studies, sulfur analyses, and bulk chemical analyses of selected elements by atomic absorption spectroscopy (AAS) and anodic stripping voltammetry (ASV) following total dissolution. Oxidation of sulfides is retarded by the core preservation method described in the "Introduction" section (this chapter).

Visual Core Descriptions

Sulfide rocks were described using the visual core description (VCD) form for igneous and hydrothermally altered rocks (see "Igneous Petrology and Geochemistry" and "Hydrothermal Alteration" sections, this chapter), which has been modified to accommodate sulfide rocks. All visual descriptions were entered into a computerized database for sulfide rocks. This form was completed for each lithologic unit and contains the following information:

1. leg, site, hole, core, type, section, and piece number;
2. major minerals, abundance, and characteristics;
3. minor minerals and characteristics;
4. trace minerals;
5. textural description;
6. structures (i.e., veins, fractures, size, orientation); and
7. sketches, comments, etc.

A classification system was established based on the macroscopic descriptive attributes of the samples. Each rock type is defined by its content of principal minerals, as determined by hand sample examination, and its most prominent textural attributes. The mineral content and textural characteristics of representative samples of each type were confirmed using polished thin section data. The principal opaque minerals pyrite (includes marcasite), chalcopyrite, and sphalerite (includes wurtzite) and the nonopaque minerals quartz (includes chalcedony and amorphous silica), anhydrite, and amorphous Fe-oxides (referred to as "gangue minerals" by sulfide petrologists) are generally distinguishable macroscopically. Gangue minerals typically fill veins, fractures, pore spaces, and cavities in sulfide aggregates; they also occur as discrete grains disseminated throughout the sulfides or intimately intergrown with sulfides. By convention, major constituents are >10 vol% and minor constituents are <10 vol%.

Determination of sulfide textures is more subjective. Various terms used conventionally by sulfide petrologists are defined in Table 1. The determination of "grain size" refers primarily to the size of mineral aggregates and not to individual grains or crystals. For the purposes of Leg 158, "very fine grained" refers to either individual sulfide or oxide grains or aggregates of 0.5 mm diameter or less, "fine grained" to grains or aggregates between 0.5 mm and 1 mm, "medi-

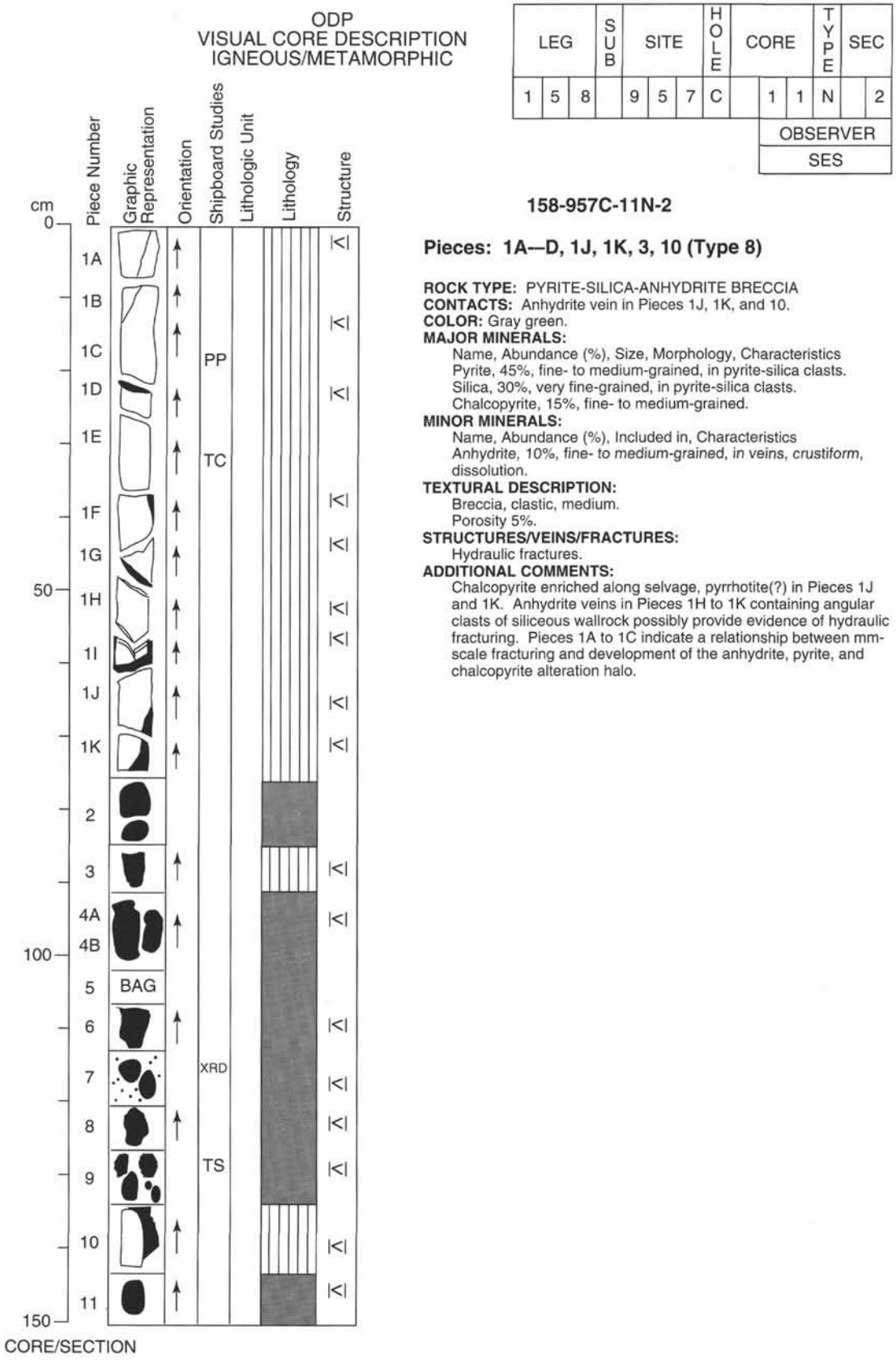

Figure 3. Example of hard-rock visual core description form used during Leg 158.

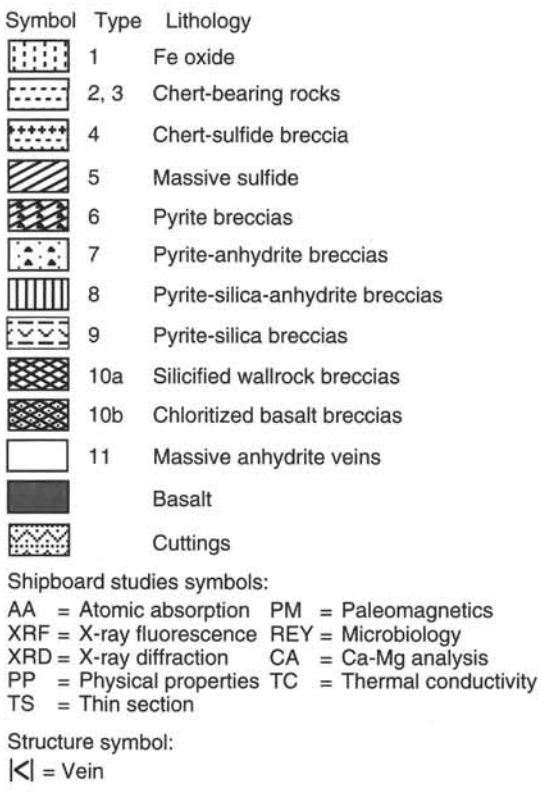

Figure 4. Key to symbols used in "Graphic Lithology" column on the core description form shown in Figure 3.

um grained" to grains or aggregates between 1 and 2 mm, and "coarse grained" to grains or aggregates of more than 2 mm (Table 2). The grain size of the silicate and nonsilicate minerals is usually indeterminate macroscopically, except where obvious vein-filling or cavity-filling is evident. Sulfate grain sizes generally refer to individual grains. Grain shapes for individual crystals are described as anhedral, subhedral, or euhedral (also idiomorphic). Special mention is made of relationships between sulfide minerals as these observations are the basis for establishing a detailed paragenesis. Certain of these textures are process-related and include cementation, replacement, dissolution, and reprecipitation.

The various sulfide types are determined without any particular reference to stratigraphic relationships, and the major characteristics of the different types are summarized in Table 3. This classification system is meant to account only for the sulfide-bearing rocks obtained on Leg 158. Occasionally, a sample will not fit all the subtype criteria as listed in Table 3 and will be given the "family" designation, such as "Type 5 Massive Sulfide" or "Type 7 Pyrite-Anhydrite Breccia." Mineralogical and textural features of sulfides found in other sites, including sedimented ridges (see Leg 139), are at least in part different from those obtained on Leg 158. Mineral abundances listed in Table 3 are approximate and meant to serve only as a guide for identification of different sulfide types. Mineral abundances within individual sulfide types may vary widely (see "Site 957" chapter, this volume). Sulfide-bearing breccias are an important sulfide type in the TAG mound, and textural terms appropriate to the description of breccias are summarized in Table 1. Breccia clasts are categorized according to size as coarse (>2 cm), medium (0.5–2 cm), and fine (<0.5 cm). Clast modifiers include the major hydrothermal minerals such as pyrite, sphalerite, chalcopyrite, silica, and Fe-oxide. By convention, the first mineral phase in the breccia name identifies the dominant clast type, and subsequent mineral names identify the dominant matrix minerals (see Table 3). Many of the clasts potentially include material precipitated directly from hydrothermal fluids, both on and below the seafloor, as well as rebrecciated sulfides that have been veined and partially replaced by other minerals. Breccia types in Table 3 are classified on the character and proportion of both clasts and matrix; for example, the distinction of pyrite-silica breccias (Type 9) and silicified wallrock breccias (Type 10). Pyrite-silica breccias contain <50 vol% basalt or silicified wallrock clasts, whereas silicified wallrock breccias contain >50 vol% basalt or silicified wallrock clasts. The term "wallrock" is used instead of basalt as the brecciated material may not strictly be basalt and may include many generations of older rock types (e.g., rebrecciated pyrite-silica breccia) with no recognizable basalt clasts.

Sulfide Log Spreadsheet

Descriptions were also entered into a sulfide log spreadsheet (see SULFLOG on CD-ROM, in back pocket). Completed spreadsheets are included with the hole summaries (see back-pocket foldout). Cataloging information for each hole, core, section, piece or bin number top, bottom, and length conforms with the other spreadsheets used during Leg 158. Each line of the spreadsheet represents a separate piece or bin in the core tray. "Type" refers to the major categories of the sulfide samples and hydrothermal precipitates as described in Table 3. "%ppt" refers to the proportion of each piece or bin that is hydrothermal in origin. "Texture" columns are used to describe the major textures, in order of proportion, using terms listed in Table 1. An "X" in the "Thin" column refers to whether information has been supplemented using a thin/polished section. "Porosity" of the sample is estimated visually, and the character of the porosity is classified as "V" for open pore spaces or vugs >5 mm and "P" for finer grained pore spaces. Mineral abbreviations are given in Table 4. In hand specimens, all FeS_2 is reported as pyrite, all ZnS as "Dark" sphalerite, and all SiO_2 as quartz. Distinction between pyrite and marcasite, sphalerite and wurtzite, and amorphous silica, chalcedony, and quartz was made only if a thin/polished section was described. In thin section, yellow or orange sphalerite (when viewed in transmitted light) was reported as "Light" sphalerite, and red or darker sphalerite was reported as "Dark" sphalerite. The "%" of a mineral present in hand specimen was estimated visually, except where a thin section has been used to supply additional information. By our convention, mineral abundances in the sulfide log spreadsheet total to 100%; porosity was considered separately. Grain-size classification abbreviations are described in Table 2. Wallrock material associated with sulfides was described in the "WR" column. The "%" is estimated visually and the "Description" includes information on lithology and alteration characteristics. The "Comments" column is used for any additional information describing the sample.

Polished Thin-section and Polished Section Descriptions

Polished thin sections and polished sections of sulfide sediments and sulfide rocks were examined to refine visual observations, and to document textural relationships and mineralogy in greater detail. Mineral name, mineral and void percentages, size, textural descriptions, and general comments on the different sulfides were entered into the computerized database as an ASCII file designed to emulate HRTHIN. The terminology is consistent with that used for megascopic descriptions. Polished thin-section and polished section descriptions are included in the site summary appendixes and are also available from the ODP computerized database. Table 3 (in "TAG-1" chapter) summarizes microscopic observations made from sulfide thin sections.

X-ray Diffraction Analyses

The Philips ADP 3520 X-ray diffractometer, which is normally used for the X-ray diffraction (XRD) analysis of mineral phases on board, was not available. Therefore, 75 samples were selected on

Table 1. Summary of textural terms used to describe sulfides.

MAJOR MODIFIERS OF SULFIDE TEXTURES (Texture 1)	
Massive sulfides	Rocks containing >75% sulfide minerals
Semi-massive sulfides	Rocks containing 50%–75% sulfide minerals, forming homogenous aggregates or intergrowths of sulfide minerals
Disseminated sulfides	Rocks containing between 5% and 50% disseminated sulfides
Vein and stringer sulfides	Rocks containing more than 50% sulfide veins
Sulfide breccias	Fragmental or clastic rocks consisting of more than 50% combined sulfide in the matrix and framework
Fe oxides	Rocks containing more than 50% Fe oxides
Chert	Dense amorphous silica chalcedony or cryptocrystalline quartz
Drill Cuttings	Silt, sand or gravel-sized hydrothermal precipitates of drilling induced origin
MINOR MODIFIERS OF SULFIDE TEXTURES (Texture 2 and Texture 3)	
Massive and semimassive sulfides and associated gangue minerals:	
Atoll texture	Minerals surrounded by and partially replaced by another
Banded	Precipitates showing rhythmic compositional or textural layering
Botryoidal	Aggregate of spherical shapes (also globular)
Boxwork	Network of intersecting crystals deposited in cavities formed by dissolution of other minerals
Chalcopyrite disease	Fine inclusions of chalcopyrite in sphalerite
Colloform	Finely laminated texture, usually in very fine-grained pyrite, formed by rhythmic precipitation
Crustiform	Encrustation of minerals formed by precipitation on preexisting framework
Dendritic	Mineral deposited in a branching pattern
Disseminated	Discrete grains or aggregates of a mineral distributed throughout a rock
Felted	Lath-shaped crystals interwoven in an irregular fashion
Filamentous	Minerals precipitated along microscopic fibers (possibly bacterial filaments)
Framboidal	Spheroidal aggregates of microscopic pyrite grains
Granular	Aggregates of sulfide grains or crystals with a sugary texture
Intergrown	Minerals with mutual grain boundaries and textures
Interstitial	Occupying the space between other minerals, infilling pore space
Interstices	Opening or space between minerals
Mesh network	Replacement texture forming a porous network enclosing remnants of the original mineral
Nodular	Discrete subrounded aggregates (sometimes colloform or radial mineral growths)
Poikilitic	Several small grains of one mineral included within another mineral crystal
Porphyroblastic	Recrystallized euhedral minerals within a finer grained primary matrix
Porous	Rocks with greater than about 10% of open spaces
Pseudomorph	Replacement of one mineral by another, retaining the original crystal form
Reticulate	Compare with "Mesh network"
Skeletal	Development of the outline of a crystal with incomplete filling
Veined	Crosscut by veins or another mineral
Vermicular	Wormlike intergrowths of one mineral in another
Vuggy	Rock containing coarse pore spaces (>2mm)
Additional terms applied to vein and stringer sulfides:	
Anastomosing	Mutually intersecting vein network
Barren	No sulfide minerals in vein fill
Branching	Single vein splitting into several new veins
Halo	Alteration extending outside vein into wallrock
Parallel	Two or more veins with the same orientation
Selvage	Mineral precipitation along edge of vein at contact with wallrock
Simple	Single with no irregularities
Additional terms applied to breccias and other fragmental sulfides:	
Graded	Fine-grained material on top of coarser material
Clast or framework-supported	Breccia or fragmental in which clasts are in mutual contact
Matrix-supported	Breccia or fragmental in which clasts are isolated in matrix material
Sorted	Composed of clasts of uniform size and composition
Sulfide-sulfide	Breccias with sulfide clasts and sulfide matrix
Sulfide-silicate	Breccias with sulfide clasts and silicate matrix
Silicate-sulfide	Breccias with silicate clasts and sulfide matrix
Sulfide-sulfate	Breccias with sulfide clasts and sulfate matrix
Additional terms applied to oxidized sulfides:	
Corroded	Euhedral grains showing evidence of dissolution
Gossanous	Sulfide assemblage that has altered primarily to Fe oxides
Relict grains	Remnants of sulfide grains that have been partially dissolved
Sooty	Coated in black amorphous Fe sulfides produced during oxidation
Tarnished	Coated by brightly colored secondary sulfides
Fossilized structures:	
Biogenic features	Mineralized or replaced biological debris (e.g., fossilized worm tubes, bacterial filaments)
Chimney fragments	Recognizable fragments of sulfide structures such as chimney walls

Note: Textures 1, 2, and 3 refer to column headings in the SULFLOG table on CD-ROM.

Table 2. Grain-size classifications for sulfides.

Very fine grained	vfg	<0.5 mm
Fine grained	fg	0.5–1 mm
Medium grained	mg	1–2 mm
Coarse grained	cg	>2 mm

board for shore-based X-ray diffraction analysis by one of the shipboard scientists.

Seventy-five samples were analyzed by X-ray diffraction at the Centre de Géochimie de la Surface (CNRS) of the Université Louis Pasteur of Strasbourg, France. Mineralogical composition of the 75 bulk samples by X-ray diffraction will be presented in Chapter 7 (see Table 10). The analytical conditions were as follows: Phillips-Norelco generator setting: 40 KV and 20 mA; a Cu tube with graphite monochronometer and Mn filter; scan speed: 0.02°/s; peak angle range: 3.000°–65.000°; range in d spacing: 1.43365 to 29.4267 Å; crystal peak width range: 0.00° to 2.00°; minimum peak significance: 0.75; 1° divergence slit used.

Samples were ground by hand with an agate mortar and pestle and the unoriented powders mounted in 1-cm^2 aluminum sample holders.

Data were collected on PC diskettes for further mineral identifications using a computerized ASTM (with additional diffraction data) database. Minerals were identified by comparing, for each sample, the printed listing of the d spacings and the corresponding intensity ratios with ASTM X-ray diffraction cards of reference minerals. Minerals with the highest intensity ratios were first taken into consideration until only a few peaks with low to very low intensity ratios

Table 3. Classification of Leg 158 sulfide samples and hydrothermal precipitates from Leg 158.

	Type and textural description	Sulfide minerals	Gangue minerals	Major features/comments
1.	Fe-oxides Massive, friable, crustiform Fe-oxides with high porosity	Tr. diss. sulfides	Fe-oxides, am. silica	Commonly as porous amorphous silica with Fe-oxide staining; commonly partially silicified and transitional to red chert
2.	Red chert Cryptocrystalline quartz with fine-grained inclusions of Fe-oxides	Diss. pyrite (<10%)	Quartz, am. silica, Fe-oxides ± anhydrite	Commonly with fine- to medium-grained disseminated pyrite euhedra; locally fractured and veined by late silica, anhydrite, or sulfides
3.	Gray silica Massive, porous, fine-grained silica; locally cherty and with fine-grained inclusions of disseminated sulfides	Diss. pyrite (<10%)	Quartz, am. silica, ± Fe-oxides	Some fragments may be highly altered glass or other silicified wallrock fragments
4.	Chert-sulfide breccia Clasts of red or gray chert and massive porous pyrite in a fine cherty matrix	Pyrite (≥50%) ± chalcopyrite	Quartz, am. silica, Fe-oxides	Dominantly sulfide fragments in a siliceous matrix of red or gray chert; locally with Fe-oxide or cherty clasts
5.	Massive sulfides (>75% sulfides)			
	a. Porous massive pyrite Fine-grained, dendritic to colloform pyrite; typically with >20% pore space	Pyrite (>75%) ± sphalerite ± chalcopyrite	Am. silica, anhydrite, quartz	Locally with clasts of gray silica, red chert, or Fe-oxides; locally as matrix of sulfide-cemented and locally vuggy breccias
	b. Porous massive sphalerite Fine-grained, dendritic to colloform sphalerite; typically with >20% pore space	Sphalerite (>75%) ± pyrite, marcasite ± chalcopyrite	Am. silica, quartz, anhydrite	Closely resembles white smoker chimney material from the surface of the mound
	c. Massive granular pyrite Fine- to medium-grained, dense, granular pyrite; locally recrystallized to coarse-grained aggregates	Pyrite (>75%) ± sphalerite ± chalcopyrite	Am. silica, quartz, anhydrite	Commonly as clasts within pyrite-silica or pyrite-anhydrite breccias
	d. Massive chalcopyrite Very fine- to fine-grained, porous chalcopyrite; coarse-bladed crystals; massive aggregates	Chalcopyrite (>75%) ± pyrite ± marcasite ± sphalerite	Anhydrite	Closely resembles chimney and sulfide crust material from the surface of the mound
6.	Massive pyrite breccias (>75% pyrite, <10% matrix)			
	a. Porous, nodular pyrite breccia Nodular pyrite clasts in a porous, sandy pyrite matrix with minor anhydrite or silica	Pyrite (>75%) ± chalcopyrite	Anhydrite ± quartz	Dominantly clast-supported
	b. Massive pyrite breccia (vein-related) Dominantly coarse, angular massive pyrite fragments with minor silica or anhydrite matrix	Pyrite (>75%) ± chalcopyrite	Quartz, anhydrite	Typically as brecciated massive pyrite veined by anhydrite; along margins of large anhydrite veins
7.	Pyrite-anhydrite breccias (>10% anhydrite matrix)			
	a. Massive pyrite-anhydrite breccia Angular fragments of massive pyrite in a matrix of anhydrite	Pyrite (50–75%) ± chalcopyrite	Anhydrite, quartz	Typically framework-supported
	b. Nodular pyrite-anhydrite breccia Modular pyrite clasts in a matrix of anhydrite	Pyrite (≤50%) ± chalcopyrite	Anhydrite, quartz	Dominantly matrix-supported
	c. Nodular, siliceous pyrite-anhydrite breccia Nodular, quartz-pyrite and gray siliceous clasts in a matrix of anhydrite	Pyrite (≤50%) ± chalcopyrite	Anhydrite, quartz	Dominantly matrix-supported; siliceous clasts may be fragments of Type 9 pyrite-silica breccias (see below)
	d. Pyrite-anhydrite breccia (vein-related) Angular fragments of massive pyrite in a matrix of anhydrite	Pyrite (50–75%) ± chalcopyrite	Anhydrite, quartz	Typically as brecciated massive pyrite veined by anhydrite; along the margins of large anhydrite veins (see also Type 6b, massive pyrite breccias)
8.	Pyrite-silica-anhydrite breccia (>10% quartz and anhydrite matrix) Quartz-pyrite and gray siliceous clasts in a quartz-rich matrix with locally abundant anhydrite veining	Pyrite (50–75%) ± chalcopyrite	Quartz, anhydrite	Quartz occurs mainly as patchy gray siliceous material and may be remnants of pre-existing pyrite-silica (Type 9) or silicified wallrock (Type 10) breccias
9.	Pyrite-silica breccias (>10% quartz matrix)			
	a. Pyrite-silica breccia Quartz-pyrite and gray siliceous clasts in a quartz matrix	Pyrite (50–75%) ± chalcopyrite	Quartz, anhydrite	Quartz occurs mainly as patchy gray siliceous material and may be remnants of pre-existing silicified wallrock breccia (Type 10)
	b. Nodular pyrite-silica breccia Nodular pyrite clasts in a quartz matrix	Pyrite (<50%) ± chalcopyrite	Quartz ± anhydrite	Pyrite occurs dominantly as fine- to medium-grained disseminated and nodular aggregates in gray siliceous matrix

Table 3 (continued).

	Type and textural description	Sulfide minerals	Gangue minerals	Major features/comments
10.	Silicified wallrock breccias			
	a. Silicified wallrock breccia Coarse, siliceous wallrock fragments with disseminated pyrite in a quartz-rich matrix	Pyrite (<50%) ± chalcopyrite	Quartz ± anhydrite	Dominantly framework-supported; quartz occurs as gray siliceous material (replaced wallrock) and in veins; minor anhydrite occurs in late veins
	b. Chloritized basalt breccia Coarse, chloritic basalt fragments; commonly with clay-altered rims	Pyrite (<50%) ± chalcopyrite	Quartz, chlorite, clays	Dominantly framework-supported; locally with recognizable pillow fragments and hyaloclastite; sulfides and quartz occur mainly in veins
11.	Anhydrite veins Massive, banded, or crustiform, medium-to coarse-grained anhydrite	Pyrite (£20%) Chalcopyrite (≤10%)	Anhydrite (>75%)	Predominantly open-space filling; concentric banding around open fractures indicates multiple episodes of vein-filling; commonly with well developed pyritization halo

Notes: Tr. = trace, diss. = disseminated, and am. = amorphous.

were left in the listings; the latter were ascribed to minor or trace mineral constituents of the sample.

Atomic Absorption Analyses

Sulfide rock and sediment were sampled routinely from each section for shipboard chemical analyses. All samples were ground to minus 200-mesh in a Spex 8000 Mixer Mill (steel grinding containers). Cu, Pb, Zn, Fe, Ag, and Cd were determined on a selected suite of samples by atomic absorption spectrometry (AAS). Calibration standards for each elements were prepared by diluting 1000 ppm Fisher Scientific standards to the optimum range within the linear portion of the calibration curve. From about 50 cm^3 of sample that was ground, 1 g was weighed and dissolved in a mixture of HNO_3 and HF. The dissolution procedure was modified after Bouvier (1991) and is similar to that presented in the *Initial Reports* of Leg 139 (1992). However, no EDTA or HCl was added. At the end of the dissolution procedure, the solution was brought to a volume of 50 mL. One milliliter of this stock solution was diluted by 10% HNO_3 to 50 mL. This solution was analyzed for Cu, Zn, and Fe. The remaining stock solution was used to determine concentrations of Cd, Pb, and Ag.

Major and trace metal analyses were performed on a Varian Spectra AA-20 using an air-acetylene flame. Wavelength settings, slit width, and gas flow were controlled manually. Element concentrations were calculated automatically from the calibration curve. Two pre-analyzed massive sulfide samples (supplied by M. Hannington, Shipboard Scientific Party) were used as reference materials to test the accuracy of the analytical procedure. A list of analytical parameters used for AAS analysis is given in Table 5, and the results of analyses of the two reference samples are shown in Table 6.

Sulfur Analyses

Total sulfur analyses were conducted on a selection of the sulfide samples analyzed for transition metals by AAS. Analytical procedures are the same as those described in the "Explanatory Notes" of the Volume 139 *Initial Reports* (1992).

Gold Analyses

Gold was determined in selected sulfide samples by means of anodic stripping voltammetry (ASV) using a Chemtronics PDV-2000 Portable Digital Voltammeter. ASV is an electroanalytical method in which gold is plated from solution onto a working electrode by applying a negative potential and subsequently stripped from the electrode by applying a reverse potential. The concentration of gold in solution is determined by measuring the current produced by stripping the gold off the electrode. The method of sample preparation was modified from Hall and Vaive (1992). Two grams of powdered material were dissolved in concentrated HNO_3, evaporated to dryness, redissolved in a mixture of HCl and HNO_3, and centrifuged. Gold remaining in the final solution was extracted onto ethyl acetate, evaporated to dryness, and redissolved in HCl and HNO_3 for analysis. The recovery of gold in solution by this method was determined from analyses of a gold-bearing reference material (massive sulfide with a predetermined gold content of 3.3 ppm Au; supplied by M. Hannington, Shipboard Scientific Party). Calibration standards for gold were prepared by diluting 1000 ppm AAS standard solutions.

Structural Visual Core Description

Vein orientation data from the archive half of the drill core were entered into a structural visual core description (SVCD) form and into a structural geology log (Fig. 5). The SVCD provides one scaled column for basic core-log sketches, annotations, measured orientations and their locations, and the corrected dip direction for the specific features relative to the core reference frame (see below). All structur-

Table 4. Mineral abbreviations for sulfide and gangue phases.

Py	Pyrite
Mc	Marcasite
Po	Pyrrhotite (may be monoclinic/magnetic or hexagonal/nonmagnetic)
Cp	Chalcopyrite
Bn	Bornite
Iso	Isocubanite
Sp (D)	Sphalerite (dark, Fe-rich); possibly wurtzite if hexagonal and anisotropic
Sp (L)	Sphalerite (light, Fe-poor)
Cv	Covellite
Dg	Digenite
Cc	Chalcocite
Am SiO_2	Amorphous silica (commonly associated with bacterial filaments)
Op-A	Opal-A
Cris	Cristobalite
Qtz	Quartz
Chalc	Chalcedony
Anhyd	Anhydrite
Gyp	Gypsum
Am FeO	Amorphous Fe-oxides (commonly associated with bacterial filaments)
Goe	Goethite (also lepidocrocite; usually more massive and crystalline than amorphous Fe-oxides)
Hm	Hematite
Mt	Magnetite
MnO	Manganese oxides (birnessite, etc.)
Chl	Chlorite
Smec	Smectite
Clays	Other claylike minerals
WR	Wallrock (undifferentiated)

Table 5. List of analytical parameters for AAS analysis of sulfides.

Element	Wavelength (nm)	Slit (nm)	Background correction	Working range (ppm)	Detection limit solution (ppm)	Blank (ppm)
Fe	372.0	0.2	No	10–300	<5	<5
Cu	327.4	0.5	No	1–30	<1	<1
Zn	213.9	1.0	Yes	0.05–3	0.01	0.03
Pb	217.0	1.0	Yes	0.5–30	0.2	<0.2
Ag	328.1	0.5	No	0.1–10	<0.1	<0.1
Cd	228.8	0.5	Yes	0.5–2.0	<0.1	<0.1

al orientations are given in dip directions. Vein observations were made from both working and archive halves of the core, but measurements were taken only on the archive half (see orientation of structures below).

Where crosscutting relationships exist in a piece of core and it was possible to determine relative age relationships, veins were given subscripts that reflect the earliest to latest feature, such that V_1 is overprinted or crosscut by V_2 in the location being described. Thereafter, if it was not possible to determine relative age relationships, the veins were numbered consecutively from the top of the section and no genetic relationships were implied. Note that relative age relationships are applicable only to the section being described and not to the core interval as a whole.

Structural Measurements

Vein orientations were measured on the archive half of the core using a contact goniometer. The core reference frame was oriented such that a horizontal slice through the core contained the core axis in its center and it was assumed that the core axis was always vertical. The "pseudo-north," 000°, is at 90° to the cut face of the archive core, and the right side was designated "pseudo-east," 090° and the left side "pseudo-west," 270° (Fig. 6). All orientations were measured as dip directions. Dip directions relative to the core reference frame were calculated stereographically from two apparent dip angles measured on vertical planes or from one apparent dip angle and a strike measured on a horizontal plane. If the structure was exposed in three dimensions and the true dip and working azimuth could be measured, these were entered directly into the structural geology spreadsheet. Dip directions were calculated using the stereonet plotting program of R.W. Allmendinger, Version 4.II. Reorientation of the core reference frame to the true geographical azimuth was not possible.

Vein orientations were recorded relative to core piece and section depths. The depth was defined as the point where the vein intersects the central divide of the cut face of the archive half of the core (Fig. 6). Depths were measured from the top of the core section in centimeters. If the vein extended over a depth interval, then the top and the bottom of its range were recorded.

HYDROTHERMAL ALTERATION

Visual core description data were entered into the computerized database HARVI. To ensure accurate core descriptions, thin-section petrography was integrated with visual core descriptions where possible. The descriptions document secondary features such as veins, alteration halos, patchy alteration, and pervasive "background" alteration.

When describing rocks, the core was examined for different alteration units on the basis of changes in secondary mineral occurrence and abundance in both rocks and veins, as well as texture, grain size, rock composition, and presence and type of breccias. Such alteration units could overlap or crosscut lithologic units defined by igneous features. For each unit and section, the following information was recorded.

Pervasive "background" and patchy alteration: The data recorded include the type and degree of alteration (visual volume percent estimate) for the pervasive "background" alteration of each piece. Characterization of any patchy alteration halos includes their size, an estimate of the total percent of the host rock comprising patchy alteration, and the percent alteration of the rock within the patches.

Veins and associated alteration halos: Vein type was based on mineralogy, and the data include width and vein abundance expressed as the volume percent of the enclosing piece represented by the vein. Documentation of vein-related alteration halos includes halo type (based on color and mineralogy), abundance of secondary phases comprising the halo, halo half-width, and abundance of halos expressed as the percentage of the piece represented by the halo.

IGNEOUS PETROLOGY AND GEOCHEMISTRY

Macroscopic and microscopic observations of igneous petrography were made from the recovered core samples and from thin sections of representative samples. Observations of core samples were

Table 6. Results of AAS analysis of two sulfide reference materials.

Element	Sulfide reference A	AAS-1	Error (%)	AAS-2	Error (%)	Sulfide reference B	AAS-1	Error (%)	AAS-2	Error (%)
Fe (wt%)	22.7	22.59	2	20.55	3	29.9	31.1	3.5	30.6	3.5
Cu (wt%)	0.36	0.84	1.2	0.77	1.9	20.5	18.18	1.6	17.89	1.4
Zn (wt%)	13.7	12.01	2.1	11.09	1.5	0.01	0.088	3.0	0.085	3.0
Ag (ppm)	400	246	1.3	257	1.6	8	9.6	2.0	9.4	0.7
Pb (ppm)	900	899	1.8	852	2.5	50	12.0	20.0	21.0	21.0
Cd (ppm)	500	589	16	513	14	2	7.2	9.0	7.8	8.0

Hole	Core	Core type	Section	Piece	Top (Curatorial), cm	Bottom (Curatorial), cm	Curatorial depth, cm	Estimated depth, mbsf	Identifier	Identification no. in SVCD	Thickness (min.), mm	Thickness (max.), mm	Estimated thickness 1, mm	Estimated thickness 2, mm	Apparent dip direction 1	Apparent dip 1	Apparent dip direction 2	Apparent dip 2	Strike	Dip direction	Dip	Comments
957A	3	X	1	2	8	13	10	10			0.2	2										Irregular network 0.2 to 2 mm width fractures in red silica

Figure 5. Sample page from the structural geology log form used for Leg 158.

recorded in modified ODP "barrel sheets" for igneous and metamorphic rock description (see "Stratigraphy" section). Petrographic information was stored electronically in the ODP database using HARVI for core descriptions and HRTHIN for thin-section observations. Descriptions of the types of information recorded in the ODP HARVI and HRTHIN databases and "barrel sheets" are given in the "Igneous Petrology" section, "Explanatory Notes" chapter of the *Initial Reports* volumes for Legs 135 (Parson, Hawkins, Allan, et al., 1992), 139 (Davis, Mottl, Fisher, et al., 1992), 140 (Dick, Erzinger, Stokking, et al., 1992), and 148 (Alt, Kinoshita, Stokking, et al., 1993). In addition, spreadsheets were used to record these data in an igneous lithology log (see "Igneous Petrology and Geochemistry" section, "TAG-4" chapter) from core observations. These spreadsheets were used to provide a format for data archiving that could be manipulated.

Rock Names

By ODP convention, basalt and diabase are named according to the abundance of phenocrysts, with mineral name modifiers added to reflect the relative abundance of these phases. These rocks are termed "aphyric" if they contain less than 1% phenocrysts, "sparsely phyric" if the phenocryst abundance is 1%–2%, "moderately phyric" if there are 2%–10% phenocrysts, and "highly phyric" if the abundance of phenocrysts exceeds 10%. Mineral name modifiers are added with the most abundant phenocryst first; hence, a sparsely plagioclase-olivine phyric basalt would contain between 1% and 2% phenocrysts of plagioclase and olivine, and plagioclase would be more abundant than olivine.

Igneous Petrology Logs

The igneous lithology log (see "Igneous Petrology and Geochemistry" section, "TAG-4" chapter) lists the rock name, visual estimates of the percentages of visible grains, average grain size for phenocrysts and groundmass, phenocryst habit and shape, color, groundmass type, percentage of vesicles, percentage of glass, degree of alteration, and other comments, such as crystallinity and texture. The minerals are listed in order of abundance for phases consisting of >0.5% of the rock. This type of naming convention has been described by Dick, Erzinger, Stokking, et al. (1992) for Leg 140.

Igneous Geochemistry

Representative samples of the various lithologies from the core were analyzed for major element oxide and selected trace element

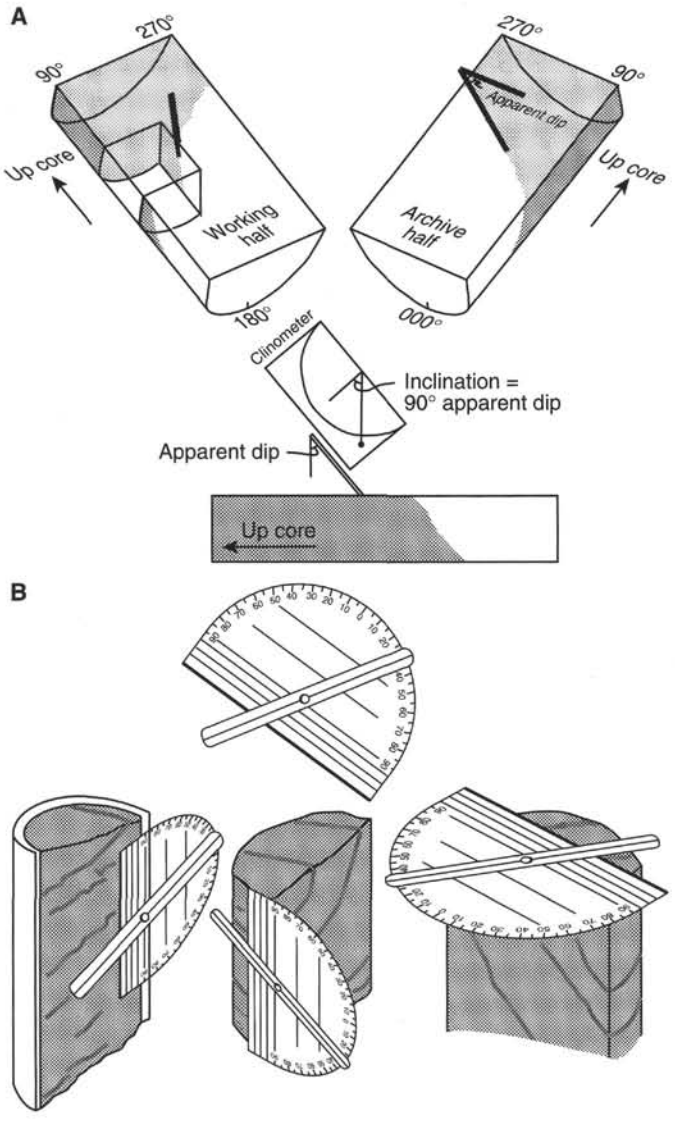

Figure 6. Diagram to show the (**A**) conventions and (**B**) tool used for measuring structural features in core during Leg 158.

compositions by X-ray fluorescence (XRF) methods. Details of the shipboard analytical facilities and methods used are given in the *Initial Reports* volumes from Legs 135 (Parson, Hawkins, Allan, et al., 1992), 140 (Dick, Erzinger, Stokking, et al., 1992), and 147 (Gillis, Mével, Allan, et al., 1993). The elements that were analyzed and the operating conditions for Leg 158 XRF analyses are shown in Table 7. Samples were powdered using a tungsten carbide shatterbox.

PHYSICAL PROPERTIES

Introduction

Physical properties data collected on board the *JOIDES Resolution* during Leg 158 provide important information that supplement the characterization of lithologic units and complement paleomagnetic studies. The physical properties measurements are made on intact full cores, on 10- to 20-cm-long half-round pieces, and on samples (minicores and fragments) extracted from the split cores. The measurements include multisensor track (MST) scanning, index properties (bulk density, grain density, porosity, and water content), compressional-wave velocity, electrical resistivity, and thermal conductivity. These measurements are described below and in the references cited. An effort was made to obtain a suite of different types of measurements on each sample type.

Multisensor Track (MST)

Several types of measurements were performed on suitable whole-round core sections using the multisensor track (MST). These measurements included wet bulk density and porosity by using the gamma-ray attenuation porosity evaluator (GRAPE; Boyce, 1976), magnetic characteristics of the sample using a magnetic susceptibility monitor, and natural gamma radiation (NGR; Hoppie et al., 1994). These measurements were done selectively during the leg depending on core recovery and condition, as accurate data can be obtained only from whole- or nearly whole-diameter samples with reference to the core liner. Necessary corrections for deviation from a full whole-round diameter of 66.1 mm are presented in Figure 7.

Index Properties

Index properties (bulk density, grain density, bulk water content, and porosity) were calculated from measurements of wet and dry sample weights and dry volumes on both fragments and minicores. For the wet measurements, samples were saturated in seawater and placed in a vacuum for 24 hr to achieve in situ wet conditions. After completion of all nondestructive physical properties measurements, the samples were dried for 24 hr at 35°C for the recovered sulfides and 60°C for the basalts. The relatively low drying temperature for the sulfide samples was necessary to prevent changes in mineralogy caused by oxidation. However, experiments with different drying durations confirmed that, even at 35°C, one day was sufficient time to dry the samples completely, because of their relatively high porosity. All measurements were corrected for salt content assuming a pore fluid salinity of 35‰.

Sample mass was determined on board ship to a precision of ±0.01 g using a Scitech electronic balance with a computer averaging system to account for ship motion. The sample mass was counterbalanced by a known mass such that only mass differentials of less than 1 g usually were measured. Volumes were determined using a Quantachrome Penta-Pycnometer, which is an instrument specifically designed to measure the volume and true density of the samples by employing Archimedes' principle of fluid displacement. The displaced fluid is helium, which assures penetration into crevices and interconnected pore spaces approaching 10^{-10} m in dimension. An initial purge time of 3 min was used to approach a helium-saturated, steady-state condition. Thereafter, sample volumes were repeatedly measured in 1 min purge intervals, until two consecutive measurements yielded volumes within 0.02 cm^3 of each other, the approximate precision of the Quantachrome Penta-Pycnometer. A reference volume was run with each group of samples. The standard was rotated between cells to check for systematic errors. Preliminary results of this procedure indicate that the pycnometer is fairly stable for a given cell inset, or sleeve. In addition, all cells of the pycnometer were calibrated daily and the O-rings of the cell lids were changed occasionally to assure continuous accuracy.

The bulk water content (w_{total}) of the sample can be determined as the ratio of pore fluid mass (M_{pf}) to total sample mass (M_{total}):

$$w_{total} = M_{pft}/M_{total} . \quad (1)$$

It is usually reported as a percentage:

$$W_{total} = w_{total} \times 100\%. \quad (2)$$

Because the pore fluids of seafloor rocks contain dissolved salts that will change phase during the drying of the sample, it is necessary to

Table 7. X-ray fluorescence operating conditions, analytical error estimates, and detection limits.

Element	Line	Crystal	Detector	Collimator	Peak angle (deg φ)	Background offset (deg 2φ)	Count time peak (sec)	Total count time background (sec)
Major elements								
SiO_2	Kα	PET (002)	FPC	Coarse	109.21	0	40	0
TiO_2	Kα	LiF (200)	FPC	Fine	86.11	0	40	0
Al_2O_3	Kα	PET (002)	FPC	Coarse	145.18	0	100	0
Fe_2O_3*	Kα	LiF (200)	FPC	Fine	57.47	0	40	0
MnO	Kα	LiF (200)	FPC	Fine	62.93	0	100	0
MgO	Kα	TLAP	FPC	Coarse	45.17	±0.80	150	150
CaO	Kα	LiF (200)	FPC	Coarse	113.12	0	40	0
Na_2O	Kα	TLAP	FPC	Coarse	55.1	–1.20	150	150
K_2O	Kα	LiF (200)	FPC	Coarse	136.69	0	100	0
P_2O_5	Kα	Ge (111)	FPC	Coarse	141.09	0	100	0
Trace Elements								
Nb	Kα	LiF (200)	Scint	Fine	21.40	–0.35	200	200
Zr	Kα	LiF (200)	Scint	Fine	22.55	–0.35	100	100
Y	Kα	LiF (200)	Scint	Fine	23.8	–0.40	100	100
Sr	Kα	LiF (200)	Scint	Fine	25.15	–0.40	100	100
Rb	Kα	LiF (200)	Scint	Fine	26.62	–0.60	100	100
Zn	Kα	LiF (200)	Scint	Coarse	41.81	–0.40	100	100
Cu	Kα	LiF (200)	Scint	Fine	45.03	–0.40	100	100
Ni	Kα	LiF (200)	Scint	Coarse	48.67	–0.60	100	100
Cr	Kα	LiF (200)	FPC	Fine	69.35	–0.50	100	100
TiO_2	Kα	LiF(200)	FPC	Fine	86.11	+0.50	40	40
V	Kα	LiF (220)	FPC	Fine	123.06	–0.50	100	100
Ce	Lα	LiF (220)	FPC	Coarse	128.13	1.50	100	100
Ba	Lß	LiF (220)	FPC	Coarse	128.78	1.50	100	100

Notes: Fe_2O_3* = total Fe as Fe_2O_3. FPC = flow-proportional counter using P10 gas. Scint = NaI scintillation counter. Trace elements analyzed at generator settings of 60 kV and 50mA; major elements, at 30 kV and 80 mA. Major elements analyzed under vacuum using goniometer 2 (1 for Na and Mg) at general settings of 30 kV and 80 mA.

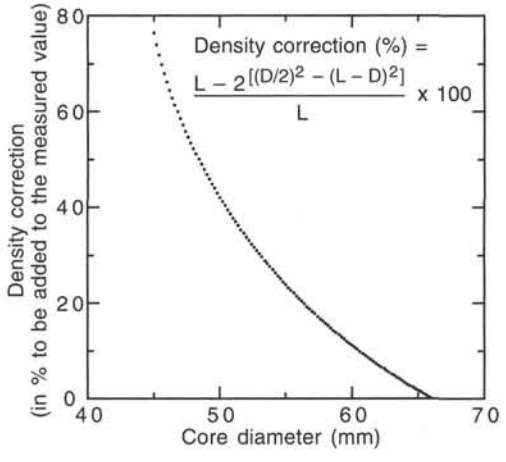

Figure 7. Estimated correction to be applied to the bulk density measurement using the GRAPE instrument to adjust for deviation of the core diameter (D) from a full whole-round diameter (L = 66.1 mm) (Boyce, 1976).

correct the water content for the salinity of the pore fluid. The salinity (s) is defined as the ratio of dissolved salt mass to the mass of the pore fluid:

$$s = M_{salt}/M_{pf}. \quad (3)$$

The drying of the bulk sample evaporates mass of pure water (M_{water}), leaving mass of precipitated salt (M_{salt}) with the mass of the solid (M_{solid}) particles. The measured dry mass (M_{dry}) therefore becomes

$$M_{dry} = M_{solid} + M_{salt}, \quad (4)$$

and the directly determined pure water mass becomes

$$M_{water} = M_{total} - M_{dry}. \quad (5)$$

The pore fluid mass (M_{pf}) is

$$M_{pf} = M_{water} + M_{salt}. \quad (6)$$

Using Equations (3), (5), and (6), the corrected pore fluid mass can be expressed as

$$M_{pf} = (M_{total} - M_{dry}) + s\,M_{pf} \quad (7)$$

and modified simply as

$$M_{pf} = (M_{total} - M_{dry})/(1 - s). \quad (8)$$

Total wet density is usually referred to as bulk density (r_{bulk}). It is defined as the total wet sample mass (M_{total}) divided by the total wet sample volume (V_{total}):

$$r_{bulk} = M_{total}/V_{total}. \quad (9)$$

Grain density (r_{grain}) is defined as the mass of the solids (mineral grains) (M_{solid}) divided by their volume (V_{solid}):

$$r_{grain} = M_{solid}/V_{solid}. \quad (10)$$

To determine the grain density by using a precision balance and the pycnometer, it is assumed that all pore fluids have evaporated from the sample after oven drying, leaving the precipitated pore fluid salts with the mineral grains of the solid matter.

The porosity of a sample is defined as the ratio of the total volume of void spaces (V_{void}) to the total wet sample volume (V_{total}):

$$\text{porosity ratio } ø = V_{void}/V_{total}, \quad (11)$$

where ø in Equation (11) is usually referred to as the porosity ratio, while total porosity (Ø) is usually reported as a percentage value:

$$\text{total porosity } \emptyset = V_{void}/V_{total} \times 100\%. \quad (12)$$

The volume of voids (V_{void}) is defined as the sum of the volume of pore fluids (V_{pf}) and the volume of air or other gases (V_{gas}) contained in the sample:

$$V_{void} = V_{pf} + V_{gas}. \quad (13)$$

Because the volume of gas cannot be measured, it is assumed that the wet sample is completely saturated with pore fluid and that

$$V_{void} = V_{pf}. \quad (14)$$

Total porosity then becomes

$$\text{total porosity } \emptyset = V_{pf}/V_{total} \times 100\%. \quad (15)$$

This can be expressed in terms of pore water content (in %), bulk density (r_{bulk}), and pore fluid density (r_{pf}), a function of pore fluid salinity,

$$\text{total porosity } \emptyset = r_{bulk}\, W_{total}/r_{pf}. \quad (16)$$

From Equation (16), it can be seen that for uniform bulk and pore fluid densities, porosity simply becomes a function of the water content. It should be noted that in Equations (11) to (16), it is assumed that all pore spaces are interconnected and fluid-saturated during determination of the bulk properties of the wet samples.

Direct measurements of bulk and grain density according to Equations (9) and (10) can sometimes be unreliable, and problems with the direct measurement of bulk densities for wet samples have been reported previously (e.g., Gillis, Mével, Allan, et al., 1993). Figure 8 illustrates the direct measurements of these quantities for sulfide samples in Holes 957B and 957C. For many samples, the value of directly measured bulk density is very close to the measured grain density. This contradicts visual observations of relatively high porosities in those samples, which would in turn predict bulk density to be considerably smaller then grain density. According to the directly measured values (Fig. 8), bulk density even appears to be higher than grain density for some of the samples, which is impossible because of the lower density of the pore fluid with respect to the densities of the solid material.

To prevent the problem of incorrect determination of these index properties, two methods exist in which one of the densities (bulk or grain) can be recalculated indirectly, by using only one of the two as the direct measurement. These methods are referred to as Method B and Method C. Method B assumes that bulk density (r_{bulk}) and grain density (r_{grain}) are calculated directly by subtracting the pore fluid mass (M_{pf}) and volume (V_{pf}) from the measured total wet sample mass (M_{total}) and volume (V_{total}). Therefore,

$$r_{grain} = M_{total} - M_{pf}/V_{total} - V_{pf}, \quad (17)$$

in which M_{pf} is calculated with Equation (8), and

$$V_{pf} = M_{pf}/r_{pf}. \quad (18)$$

Method C, on the other hand, assumes that grain density (r_{grain}) is calculated directly and bulk density (r_{bulk}) is derived indirectly by adding the pore fluid mass (M_{pf}) and volume (V_{pf}) to the measured solid sample mass (M_{solid}) and volume (V_{solid}). Therefore,

$$r_{bulk} = M_{solid} + M_{pf}/V_{solid} + V_{pf}, \quad (19)$$

in which M_{pf} and V_{pf} are calculated with Equations (8) and (18).

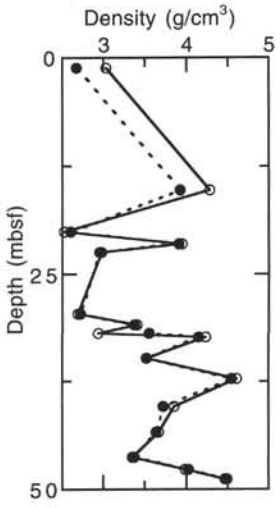

Figure 8. Directly measured bulk density (solid circles) and grain density (open circles) for samples from Holes 957B and 957C. Unreasonable values illustrate the necessity to recalculate one of the densities indirectly by using either Method B or Method C.

Accordingly, porosity can be calculated using either the bulk density of Method B or Method C and the water content.

Actual laboratory measurements on sulfide samples collected during Leg 158 make it preferable to use Method C over Method B for several reasons. Repeated measurements on dried samples led to reproducible values, whereas repeated measurements on wet samples were widely variant. Most problems occurred during volume measurements of wet samples. The time of resaturation was very crucial for the measurements. Because mass was always determined before putting the samples into the pycnometer, the amount of fluid loss in the interim was difficult to estimate. On account of the porous nature of the samples, the direct determination of the dry index properties seemed much more reliable than the direct measurement on wet samples (Fig. 8).

In the "Physical Properties" sections of the site report chapters, bulk density, grain density, and porosity values determined using Method C are mentioned in the text and plotted on the figures. For reasons of completeness, however, values for both methods are included in the index properties tables.

Compressional-wave (*P*-wave) Velocities

The pulse transmission method was employed to determine compressional-wave velocity using piezoelectric transducers as sources and detectors in a screw-press Hamilton Frame described by Boyce (1976). All measurements were made on seawater-saturated minicores (diameter = 2.54 cm, length ~ 2 cm) at zero confining pressure. The ends of minicores were carefully polished either with 240 and/or 600 grit on a glass plate to produce a right circular cylinder and to smooth the contact area. The length of each minicore was checked using a caliper along its circumference, and polishing continued until all length measurements were within ±0.02 mm. The grit was later removed by thoroughly cleaning the samples in an ultrasonic bath, before the beginning of the measurement.

Calibration measurements were performed using aluminum standard minicores to determine the zero displacement time delay inherent in the measuring system. The traveltimes through a range of different lengths of each material were measured and plotted on a time-distance graph (Fig. 9). The best fitting straight line had a linear correlation coefficient (R) very close to unity, thereby making the calibration very reliable. The intercept at zero length gives a delay time of 0.869 s for the particular set of transducers used during Leg

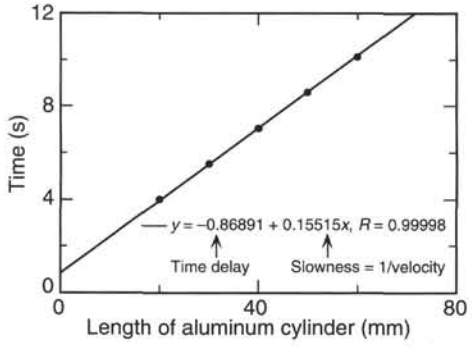

Figure 9. Calibration of the digital sound velocimeter (DSV-3) transducers by determining the delay time using aluminum standard minicores. The linear least-squares fit yields the zero length time delay and the velocity of the aluminum standard.

158. This technique is preferable to taking a single reading at zero length. The slope of the straight line fit represents the slowness of the aluminum standard. Taking the inverse yields a velocity of 6.445 km/s. The technique has been used for velocity measurements during several previous cruises and is described in the "Physical Properties" section of the "Explanatory Notes" chapter of the Volume 148 *Initial Reports* (Alt, Kinoshita, Stokking, et al., 1993). Compressional-wave (*P*-wave) velocities were measured on the newly installed (Leg 157), software-controlled, velocity-strength-resistivity device (VSR). The velocities were obtained in a direction parallel to the core axis using the digital sound velocimeter (DSV-1) for soft sediment samples, and perpendicular to the axis of the core using the Hamilton Frame system (now called DSV-3) for hard-rock minicores. Salt water was used to improve the acoustic contact between the sample and the transducers.

Electrical Resistivity

Measurements of the electrical resistivity of core samples are useful for correlation with borehole resistivity logs as well as for providing an indication of the distribution of porosity within the rock. During Leg 158, the electrical resistivity of hard-rock samples was measured on seawater-saturated minicores at room temperature and atmospheric pressure using a two-electrode cell, which was newly built on board the ship to measure resistance (R). Measurements were made at 5 V (AC) and 50 kHz frequency. The cell consists of a nylon holder and spring-loaded stainless steel holders. The holder was designed to have the same diameter as the minicores to minimize leakage along the sides of the sample. The sensors and the minicores were polished to maintain good contact. The measurements were performed on minicores with their cylindrical surfaces wrapped in Teflon tape to prevent a short circuit between the two ends of the minicores. The samples were kept saturated in seawater under low vacuum during the time period separating recovery and the making of the measurements. The minicore faces were cut smooth and parallel to allow good contact with the electrodes. Because the minicores are cylindrical in shape, we obtain the resistivity (ρ) of the sample by the equation

$$\rho = R \times S/L, \tag{20}$$

in which resistance (R) is multiplied by the instrument cell constant. The cell constant is defined for every sample as the cross-sectional surface area (S) divided by the length of the sample (L).

Thermal Conductivity

Core samples were measured nondestructively for thermal conductivity in the shipboard laboratory. Specimens were obtained from the archive half to prevent samples used for chemistry analyses from being contaminated with thermal joint compound (EG&G Type 120) used to couple the samples with thermistor probes. This procedure was previously used during Leg 148 and is documented in the "Physical Properties" section of the "Explanatory Notes" chapter of the Volume 148 *Initial Reports* (Alt, Kinoshita, Stokking, et al., 1993).

To smooth the contact area and provide good coupling with the needle probes, some of the samples required polishing either with 240 and/or 600 grit on a glass plate. This method is most suitable for the hard-rock cores, which were cut in the form of a half-round cylinder. Half-space measurements were performed over 6 min with a heated needle probe placed between the sample and a slab of low conductivity material (Sass et al., 1984; Vacquier, 1985). All half-space measurements were conducted in a seawater bath to keep the samples saturated, to improve the thermal contact between the needle and the sample, and to reduce thermal drift during the tests.

This thermal conductivity measurement method closely approximates the heating of a line source in a plane separating half spaces of the sample material and a thermal insulator. This, in turn, is an extension of the method of heating a uniform full space by a line source (Jaeger, 1956; von Herzen and Maxwell, 1959). Thermal conductivity is calculated from the rate of temperature rise in the probe while a heater current is flowing. The temperature rise in the probe should vary logarithmically with time as:

$$T(t) = (q/4\pi k)\ \ln(t) + \text{const.}, \tag{21}$$

in which k is thermal conductivity, T and t are the temperature and time, respectively, and q is heat generated per unit length of the probe. From this equation, thermal conductivity can be derived from the slope of temperature vs. the logarithm of time. If the substrate on which the sample is placed were a perfect thermal insulator, the rise in temperature with time at the needle probe would be exactly twice that experienced by the probe in an infinite medium having the same thermal conductivity as the sample. In practice, the poorly conducting substrate absorbs a fraction of the heat during measurement, the amount of which depends on the ratio of sample to substrate conductivity. For most rock samples measured during Leg 158, this ratio was sufficiently large that the adjustment from the simple theory is a relatively small correction.

The data collection and reduction procedures for half-space tests are identical to those for full-space tests. Before measuring the samples collected on Leg 158, the thermal conductivity probes were calibrated by conducting measurements on three standards of known thermal conductivities. The standards used were red rubber, macor ceramic (a slab of synthetic material), and basalt, all provided by ODP, with known thermal conductivities of 0.96, 1.61 and 2.05 W/(m·K), respectively. The needle probes were calibrated by comparing the known true thermal conductivity values of the standards with the actually observed thermal conductivities. Measurements were averaged after at least five good measurement runs for each standard and each needle probe. The probe-specific values were entered in the software, which controls the statistical analysis for each measurement run to complete the calibration. Needle 335 showed the best correlation between the true and observed thermal conductivities and was therefore preferably used for measurements (Fig. 10).

All sample measurements were carefully monitored to achieve reproducible thermal conductivity values. After a good sample-probe contact was established, the results were accepted as good data only when at least three measurements with very little drift and similar values were completed. The thermal conductivity of the sample was

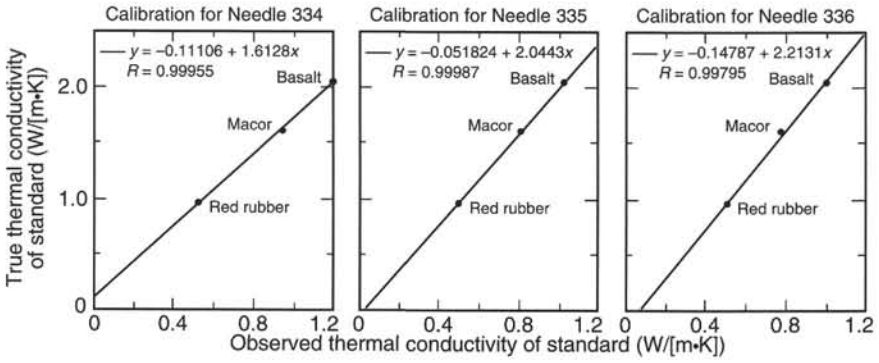

Figure 10. Calibration of thermal conductivity needle probes using three standards (red rubber, macor ceramic, and basalt) with known thermal conductivity. The linear least-squares fit between true and observed thermal conductivity is used to correct the raw data of the probes. The linear correlation coefficient (R) provides an indication of the accuracy of the probe. Needle 335 showed the best fit and was therefore preferentially used for measurements.

then determined by averaging the values obtained during those runs, including the margin of error.

PALEOMAGNETISM

Paleomagnetic measurements were performed on vertically oriented minicore samples and unoriented pieces, chosen to be representative of the lithology and alteration mineralogy of the Leg 158 cores. A standard 2.5-cm diameter minicore sample was generally taken from each section of core for shipboard study. An effort was also made to select samples near important structural features for possible reorientation using the remanent magnetization directions. The azimuths of core samples recovered by rotary drilling are not constrained. Therefore, all magnetic data are reported relative to the following core coordinates: +X (north) is into the face of the working half of the core, +Y (east) points toward the right side of the face of the working half of the core, and +Z is down (Fig. 11).

The remanent magnetization of continuous core pieces was measured with the 2G Enterprises (Model 760R) pass-through cryogenic rock magnetometer, operated in flux-counting mode. The superconducting quantum interference device (SQUID) sensors in the cryogenic magnetometer have a response function that is ~20 cm long. Declination and inclination data are derived from the effective measurement volumes for the three orthogonal sensors. An alternating field (AF) demagnetizer (Model 2G600), capable of producing an alternating field up to 25 mT, was used on-line with the pass-through cryogenic magnetometer. The natural remanent magnetization (NRM) and the remanence after demagnetization (typically at 10 and 20 mT) were measured for all archive core sections.

Most discrete samples were stepwise demagnetized using the Schonstedt AF demagnetizer (Model GSD-1). The sample was either demagnetized along the positive axis directions (+X, +Y, +Z) or the reverse axial directions (–X, –Y, –Z) at alternate demagnetization steps to facilitate recognition of any spurious anhysteretic remanence. A small number of samples were also thermally demagnetized, using the Schonstedt thermal specimen demagnetizer (Model TSD-1). Initial susceptibility was monitored between each temperature step as a means of assessing any irreversible mineralogical changes associated with heating.

Whole-core magnetic susceptibility (k) was measured at 3-cm intervals on selected sections using the Bartington Instrument susceptibility meter (Model MS1, 80-mm loop, 4.7 kHz, SI units) mounted on the multisensor track. Susceptibility measurements were made on the whole core following the establishment of the final curated positions and placement of spacers and are therefore directly comparable with the pass-through measurements of the archive half cores. The volume susceptibility of minicores was measured using the Kappabridge KLY-2. Susceptibility values on the Kappabridge are reported relative to a nominal volume of 10 cm^3; all discrete sample susceptibilities reported here have been corrected for the calculated cylindrical sample volume. The volume susceptibility was used in conjunction with the NRM intensity to calculate the Koenigsberger ratio (Q, the ratio of remanent to induced magnetization) of the samples. The IGRF field value at the TAG site (42,000 nT = 33.44 A/m) was used for calculating Q (Q = NRM [A/m]/(k [SI] × H [A/m]), where H is the local geomagnetic field).

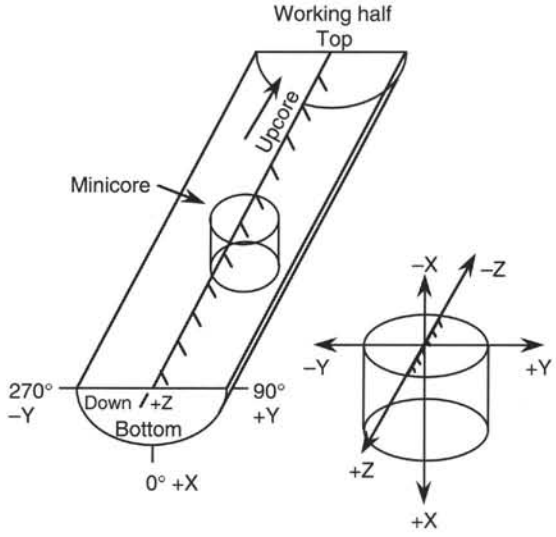

Figure 11. Orientation conventions for minicore samples.

The anisotropy of magnetic susceptibility (AMS) was determined for most shipboard samples, using the Kappabridge and the program ANI20 supplied by Geofyzika Brno. A 15-position measurement scheme was used to derive the susceptibility tensor (k_{ij}) and associated eigenvectors and eigenvalues. In addition to standard paleomagnetic measurements, a small number of minicores from the Leg 158 cores were given an anhysteretic remanent magnetization (ARM) and/or a stepwise isothermal remanent magnetization (IRM) acquisition. The ARM was generated in an alternating field of 100 mT with a bias field of 0.1 mT. The IRM acquisition experiments (to a peak field of ~1.2 T) were accomplished using the ASC impulse magnetometer (Model IM-10).

FLUID GEOCHEMISTRY

Interstitial water was obtained by in situ extraction using the water sample temperature probe (WSTP) and from sediments by squeezing.

In Situ Extraction

Borehole water was sampled using the WSTP, which simultaneously measures temperature (Barnes, 1988). The WSTP tool is lowered on the wireline to the end of the drill string, where it locks onto an assembly just above the bit. While the tool descends, the hole is flushed with drilling fluid (usually surface seawater), with the bit just off bottom to keep the hole free of fill. After the sampler is latched into place, the filter assembly projects about 1 m past the bit. A timer-operated valve opens and borehole water is drawn under negative pressure through the filter and into the sampler.

The filter assembly was lengthened to 22 cm for Leg 139 and is described in Shipboard Scientific Party (1992). The modified instrument is narrower than an earlier version of the tool. These modifications produce a filter surface area of 200 cm^2. After passing through the filter assembly, fluids enter the sample reservoir by way of 1.6 mm titanium tubing. The tube is held in a groove cut into a titanium sleeve that fits around the thermistor probe shaft. The sleeve, tubing, and filter are covered by a second titanium sleeve. This outer sleeve provides support and abrasion protection for the filter, and is perforated approximately every centimeter with 0.5 cm holes to allow fluid to pass. The titanium tube holds less than 4 mL of fluid and is connected to a titanium sample coil that holds 10 mL of fluid. A one-way valve is connected to the other end of the titanium coil, which allows fluid to pass into a stainless-steel overflow cylinder. This overflow cylinder generates negative pressure when the sampling valve is open, as this cylinder is normally filled with air when the tool is sent downhole. Before being deployed, the fluid path is back-filled with distilled water and the overflow cylinder is exposed to atmospheric pressure. A timer is set for a fixed period after which the valve will open, exposing the sampling line and chamber to ambient pressure. The timer also closes the valve after a predetermined interval has passed. The length of time required to fill the WSTP is unknown, but the valve is kept open for about 10 min. The tool is recovered after the sample valve has closed. A check valve below the sample coils maintains fluid pressure at 690 kPa (1000 psi).

When the tool is returned to the lab, the cover for the chamber containing the sample coils is carefully removed and any "overflow" water present is collected and designated as "OF" sample. This fluid includes the distilled water that occupied the space inside the titanium tubing before deployment, plus all fluid in excess of 10 mL collected downhole. If a small fluid sample (<10 mL) is collected by the tool, the overflow fluid will be nearly all distilled water, and the sample will be diluted. If a large volume is collected (>10 mL), then the fluid trapped in the sample coils is from the borehole. Fluids from the overflow cylinder were also analyzed, as they often are useful for determining the concentration of the major and minor species that are dissolved in sampled waters. In particular, this fluid sometimes shows higher alkalinity- and calcium-to-chloride ratios than the undiluted sample from the titanium coil, indicating that calcium carbonate has probably precipitated in the latter. The amount of dilution of the overflow aliquot can usually be determined from its chlorinity relative to that of the undiluted sample. Fluid from the titanium sample coil was filtered (0.2 µm) and used for determination of major and minor dissolved species.

Squeezing

Interstitial water (IW) was squeezed from one 10-cm-long, whole-round section of sediment core. Sediment from the IW whole round was immediately extruded from the core liner and scraped with a teflon-coated stainless-steel spatula to remove the outer, contaminated layer. The uncontaminated layer was placed in a titanium squeezer similar to the steel squeezer designed by Manheim and Sayles (1974). The squeezer and samples were handled with plastic gloves to avoid contamination. Sediments were squeezed in a Carver hydraulic press at pressures up to 276 MPa (40,000 psi). Interstitial water was collected directly from the squeezer into a 50-mL all-plastic syringe, from which the various aliquots for analysis were ejected through an on-line, 0.2-µm, polysulfone filter mounted in a Gelman "acrodisc" disposable filter holder. No attempt was made to equilibrate the sample with the in situ temperature before squeezing. The squeezed interstitial water was designated "IW" sample.

Analytical Methods

Interstitial fluid samples were analyzed immediately upon recovery for pH, alkalinity by potentiometric titration, and salinity by refractive index. Aliquots were refrigerated and analyzed within a few days for chlorinity, calcium, and magnesium by titration and silica, phosphate, and ammonium by colorimetry. In addition, calcium, magnesium, potassium, sodium, and sulfate were determined by ion chromatography (IC) using a Dionex DX-100. Samples were prepared as 1/200 dilutions. Instrumental calibration used variable dilutions of IAPSO. Ion Pac AS4 and Dionex CS12 columns were used for anion and cation analysis, respectively. Most shipboard analyses were performed using standard ODP techniques, as detailed by Gieskes et al. (1991). Silica, phosphate, and ammonium analyses employed primary standards made from reagent grade chemicals, with IAPSO run as an unknown. IAPSO (Cl = 19.3745 g/kg) was used as a primary standard for determination of calcium, magnesium, chlorinity, sodium, potassium, and sulfate. Analytical error for each ion measured was pH = 1.3%, alkalinity = 1.2%, salinity = 0.3%, potassium = 1.1%, magnesium = 1.6%, calcium = 0.9%, chloride = 1.4%, sulfate = 2.9%, phosphate = 5%, ammonia = 6%, and silica = 6%.

MICROBIOLOGY

Sample collection for microbiological analyses was designed so that the samples obtained had minimal chance of contamination. They were therefore collected as aseptically as possible and processed as soon as possible after collection of samples. Two types of samples were taken: (1) whole-round cores (individual pieces collected before sectioning), and (2) approximately 15-cm^3 samples from cores that recovered unconsolidated mud. Sampling distribution was biased toward the upper 50 m of the holes.

Individual pieces were obtained as soon as possible after the core arrived on the ship. The cores were brought into the laboratory and washed in sterile artificial seawater. The areas exposed to possible contamination were removed aseptically using a sterile scalpel. Hard samples were first crushed in sterile aluminum foil. Both crushed sulfide samples and muds were subsampled and treated as follows for shore-based studies:

1. Inoculation of media (for sulfur reducers and methanogens) for enrichment of hyperthermophiles.
2. Total cell counts (in 4% formaldehyde in sterile seawater, stored at 4°C).
3. Light and scanning electron microscopy (in 4% formaldehyde in sterile seawater, stored at 4°C).
4. DNA analyses (quick frozen in liquid nitrogen or stored in 80% ethanol and kept at –20°C). and
5. Enrichment of hyperthermophiles once shore-based (stored anaerobically at 4°C under nitrogen).

REFERENCES

Alt, J.C., Kinoshita, H., Stokking, L.B., et al., 1993. *Proc. ODP, Init. Repts.*, 148: College Station, TX (Ocean Drilling Program).

Barnes, R.O., 1988. ODP in-situ fluid sampling and measurement: a new wireline tool. *In* Mascle, A., Moore, J.C., et al., *Proc. ODP, Init. Repts.*, 110: College Station, TX (Ocean Drilling Program), 55–63.

Bouvier, J.-L., 1991. Total dissolution method for rock samples. *MRD/ACS, Geol. Surv. Can., Internal Tech. Rep.*

Boyce, R.E, 1976. Definitions and laboratory techniques of compressional sound velocity parameters and wet-water content, wet-bulk density, and porosity parameters by gravimetric and gamma ray attenuation techniques. *In* Schlanger, S.O., Jackson, E.D., et al., *Init. Repts. DSDP,* 33: Washington (U.S. Govt. Printing Office), 931–958.

Davis, E.E., Mottl, M.J., Fisher, A.T., et al., 1992. *Proc. ODP, Init. Repts.,* 139: College Station, TX (Ocean Drilling Program).

Dick, H.J.B., Erzinger, J., Stokking, L.B., et al., 1992. *Proc. ODP, Init. Repts.,* 140: College Station, TX (Ocean Drilling Program).

Gieskes, J.M., Gamo, T., and Brumsack, H., 1991. Chemical methods for interstitial water analysis aboard *JOIDES Resolution. ODP Tech. Note,* 15.

Gillis, K., Mével, C., Allan, J., et al., 1993. *Proc. ODP, Init. Repts.,* 147: College Station, TX (Ocean Drilling Program).

Hall, G.E.M., and Vaive, J.E., 1992. Determination of gold in geological samples by anodic stripping voltammetry at field locations. *Chem. Geol.,* 102:41–52.

Hoppie, B.W., Blum, P., and the Shipboard Scientific Party, 1994. Natural gamma-ray measurements on ODP cores: introduction to procedures with examples from Leg 150. *In* Mountain, G.S., Miller, K.G., Blum, P., et al., *Proc. ODP, Init. Repts.,* 150: College Station, TX (Ocean Drilling Program), 51–59.

Jaeger, J.C., 1956. Conduction of heat in an infinite region bounded internally by a circular cylinder of a perfect conductor. *Aust. J. Phys.,* 9:167–179.

Manheim, F.T., and Sayles, F.L., 1974. Composition and origin of interstitial waters of marine sediments based on deep sea drill cores. *In* Goldberg, E.D. (Ed.), *The Sea* (Vol. 5): New York (Wiley Interscience), 527–568.

Parson, L., Hawkins, J., Allan, J., et al., 1992. *Proc. ODP, Init. Repts.,* 135: College Station, TX (Ocean Drilling Program).

Sass, J.H., Kennelly, J.P., Jr., Smith, E.P., and Wendt, W.E., 1984. Laboratory line-source methods for the measurement of thermal conductivity of rocks near room temperature. *U.S. Geol. Surv. Tech. Rep.,* 84–91.

Shipboard Scientific Party, 1992. Explanatory notes. *In* Davis, E.E., Mottl, M.J., Fisher, A.T., et al., *Proc. ODP, Init. Repts.,* 139: College Station, TX (Ocean Drilling Program), 55–97.

Vacquier, V., 1985. The measurement of thermal conductivity of solids with a transient linear heat source on the plane surface of a poorly conducting body. *Earth Planet. Sci. Lett.,* 74:275–279.

Von Herzen, R.P., and Maxwell, A.E., 1959. The measurement of thermal conductivity of deep-sea sediments by a needle-probe method. *J. Geophys. Res.,* 64:1557–1563.

Ms 158IR-105